Self-regenerated silk fibroin with controlled crystallinity for the reinforcement of silk

David Chelazzi *,[1], Diego Badillo-Sanchez [1], Rodorico Giorgi, Alessandra Cincinelli, Piero Baglioni *

Department of Chemistry "Ugo Schiff" and CSGI, University of Florence, Via della Lastruccia 3, 50019, Sesto Fiorentino, Florence, Italy

HIGHLIGHTS

- Composite materials of self-regenerated silk fibroin (SRSF) and aged silk fibers were prepared.
- The crystallinity of SRSF films varies with the fibroin dispersions concentration.
- *In-situ* formed composite materials recover the mechanical properties of aged silk.
- Amorphous SRSF films produce composite materials with optimal mechanical properties.
- SRSF films candidate as green, sustainable consolidants for historical silk.

GRAPHICAL ABSTRACT
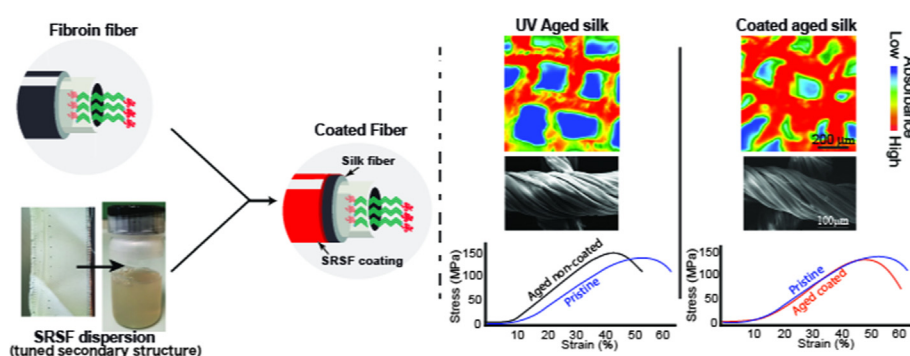
ABSTRACT

Hypothesis: Silk artifacts constitute a fundamental cultural and historical heritage, yet they are affected by degradation that alters the secondary structure of fibroin and weakens the mechanical properties of textiles, hindering their conservation. Feasible and compatible consolidants for silk are still widely needed.

Experiments: Here, we propose a robust and reliable method to restore the mechanical properties of fragile, aged silk fibers, based on the adhesion of self-regenerated silk fibroin (SRSF) with controlled crystallinity, prepared from waste silk, to the aged fibers. By varying the concentration of fibroin dispersions, the content of crystalline and amorphous domains in SRSF films can be tuned, as demonstrated by 2D micro-Fourier transform infrared spectroscopy Imaging and thermal analysis.

Findings: The presence of amorphous fibroin domains, distributed between the aged silk fibers, completely recovered their mechanical properties. Instead, the presence of domains with high content of ordered structures, distributed between the fibers, reduced their tensile strength and elongation length. The different mechanical behavior is likely due to the fact that adhesion of crystalline layers produces a brittle material, while amorphous layers with higher fibroin chain mobility increase ductility. The tunability of this treatment allows easy control of desired mechanical properties of degraded silk fibers, simply controlling the crystallinity Vs amorphousness of SRSF; these findings open up new perspectives in textile conservation, in the engineering of biomaterials and materials, and in the preparation of composite materials with enhanced properties.

© 2020 Elsevier Inc. All rights reserved.

---

* Corresponding authors.
  E-mail addresses: chelazzi@csgi.unifi.it (D. Chelazzi), baglioni@csgi.unifi.it (P. Baglioni).
[1] These authors contributed equally.

1. Introduction

Silk has been employed by mankind since ancient times to produce different types of artifacts, tapestries, and garments [1,2]. The most frequently used raw material is the domesticated B*ombyx mori* cocoon's spun fiber, which undergoes a degumming process to remove the coating of sericin [3]. The resulting silk fibers have a hierarchical structure, with filaments that are typically 7–12 μm wide, composed of fibrillar elements (ca. 1 μm wide), which in turn consist of 10 nm wide microfibrils [4]. Degummed silk is mainly composed of Heavy-Fibroin, Light-Fibroin, and P25 (a chaperonin-like protein), in a 6:6:1 ratio [5], present as amorphous and crystalline domains oriented along the fiber axis [2,6]. The composition and structure of this proteinaceous material confer to silk its valuable physical and mechanical properties, i.e. strength, resistance, lightness, smoothness and luster, which explain its use in ancient and modern fabrics, as well as in newly developed bio-materials [7–13].

Historical silk objects are an invaluable cultural and artistic heritage, which mainly includes clothes, tapestries, flags, banners and decorative objects. However, silk is affected by several degradation pathways, e.g. oxidation, hydrolysis, chain scission and chain rearrangements, mainly induced by environmental factors (relative humidity, light, temperature), and by the presence of acids, oxidizing compounds, metal components, and biopollutants [1,8,14]. The resulting changes in the secondary structures of silk fibers cause the alteration of their mechanical properties [15,16], and, consequently, historical samples can be fragile and exhibit poor flexibility [17–19]. Feasible and reliable methods to consolidate weakened silk artifacts are still strongly needed, in order to avoid the loss of this heritage.

The traditional textile conservation practice includes the use of repairs and lining, and of synthetic polymers (adhesives, glues, etc.). Repairs, such as the introduction of new silk or paper elements, are used to provide mechanical support to weakened silk objects [20–22]. However, these methods introduce non-original components in the artifacts, and do not provide the *in situ* reinforcement (at the micro scale) needed by the original fibers, which are still exposed to degradation processes. Synthetic polymers (e.g. acrylates, vinyl acetates, epoxy resins) are widely used as consolidants owing to their good adhesion and mechanical properties [23], however these materials present several drawbacks. Natural aging can cause the discoloration (yellowing) of the polymers, altering the appearance of the textiles. Vinyl polymers undergo deacetylation and loss of organic acids [24] that are detrimental to silk. Besides, aging produces changes in the molecular weight of synthetic polymers due to cross-linking or chain scission reactions that affect the polymers solubility in their original solvents, hindering their safe removal from the artifacts [25–28]. Huang et al. used epoxide-ethylene glycol diglycidyl ether (EGDE) to crosslink with tyrosine and lysine in amorphous domains of silk fibroin, and achieved mechanical strengthening [29]; previously Cai et al. had modified silk fibers with a silicone-containing epoxide, producing significant changes in the physical and chemical properties of the fibers [30].

Alternatively, biopolymers represent an attractive and sustainable source of potential consolidants for silk. Cellulose has been widely employed to formulate composites with silk fibroin [31–35], mainly to produce films, membranes, foams, and gels of biomaterials for *in vivo* use. For instance, cellulose nanofibrils (CNFs) are promising candidates owing to their strength and biocompatibility [31,36], and cellulose is able to form strong hydrogen bonds, electrostatic interactions and covalent bonds with fibroin, inducing structural changes (e.g. increase of β-sheets and decrease of random coils) in blended cellulose-fibroin films [37,38]. Bacterial cellulose films have been recently adopted by Wu et al. to reinforce ancient silk fabrics, with promising results [28]; however the process involves some time-consuming steps (bacteria culturing and extraction) and the need to efficiently remove the bacteria so as to avoid potential damage to the silk fibers.

In principle, fibroin is the ideal consolidant for silk as it grants full physico-chemical compatibility, and its application does not involve the introduction of foreign components into silk objects. Self-regenerated silk fibroin (SRSF) can be obtained and processed through a variety of methods [39–42]. Composites of fibroin (from silkworm cocoons) and silk have been extensively explored in the framework of biomaterials and materials engineering, and are typically meant to be significantly stronger than pristine natural silk [43–47]. For instance, Yuan et al. embedded silk fibers into SRSF matrices (0.2 mm thick), and observed that by increasing the amount (wt%) of fibers it is possible to obtain a significant enhancement of the films' mechanical properties [43,46]. Wojcieszak et al. investigated the behavior of pristine fibers either mono-reinforced with small amounts of films, or embedded in thicker film matrices (up to ca. half centimeter). The film processing method (filtration, evaporation temperature) was shown to affect the order of the resultant matrix, as qualitatively observed through Raman spectroscopy by measuring the full width at half maximum (FWHM) of amide I and amide III bands, and the presence or disappearance of bands in the 1100–800 cm^{-1} region (associated with β-sheets and CH_3 deformations). Composites with thicker and disordered matrices showed the highest enhancement of mechanical behavior as compared to natural silk [45].

In the present contribution, we propose a new sustainable method, based on the use of renewable silk scraps, to restore the mechanical properties of fragile (aged and degraded) silk fibers, meant for the treatment of historical objects. Specifically, the main goals of the new silk treatment are: 1) avoid embedding the fibers in thick coatings, so as to preserve the aesthetics of the treated artifacts; instead, we formulated fibroin films able to adhere homogeneously to the fibers surface, forming new film-fiber interfaces and modifying the adhesivity between the fibers to improve their mechanical properties; 2) restore the mechanical properties of aged/historical silk back to those of pristine natural silk, rather than obtain 'super strong' fibers with highly enhanced mechanical behavior; 3) achieve the controlled tuning of the secondary structure of the SRSF, in particular of the relative amount of crystalline structures, by playing on the concentration of the SRSF precursor solutions. This point is based on the following rationale: crystalline SRSF films (e.g. combined amount of β-sheets and β-turns > 60%) are expected to increase the fibers' hardness or stiffness, while the presence of highly amorphous films with higher fibroin chains mobility (e.g. β-sheets + β-turns < 30%), at the interface with the aged/degraded fibers, might increase the fibers' elongation. Recovering the ductility of the fibers is particularly desirable for brittle historical textiles where the original amorphous component was lost to degradation [17,48]. On such samples, improved elongation is needed to allow handling during the exhibition and restoration of the artifacts, as well as to increase the lifespan of the objects.

SRSF films can be obtained from waste silk textiles, rather than silkworm cocoons, with a sustainable and inexpensive approach based on the responsible use of bioresources [49]. The use of SRSF films for the consolidation of aged silk fibers is of crucial interest, since, as we demonstrate in the present contribution, the crystallinity Vs. amorphousness of the films can be tuned to obtain desired mechanical properties of the fibers. The SRSF films, cast from dispersions, were studied with Fourier Transform Infrared (FTIR) 2D Imaging, to characterize the secondary structure of the

films, and with scanning electron microscopy (SEM); then, SRSF dispersions were applied onto artificially aged silk fibers, and the same analytical set was used to investigate the distribution of the coatings on the fibers. Finally, the mechanical behavior of the treated fibers was studied through tensile strength tests, and compared to that of pristine silk.

2. Materials and methods

2.1. Chemicals used

Nitric acid (HNO$_3$, 90% ACS, Sigma Aldrich), ethanol (EtOH, anhydrous, analytical grade, Carlo Erba), and calcium chloride (anhydrous CaCl$_2$, $\geq$ 99.9%, Sigma Aldrich) were used as received. MilliQ water (resistivity 18.2 MΩ cm) was used for the experiments.

2.2. Pristine and aged silk samples

A commercial non-dyed modern silk textile (Georgette Silk) with a density of 51 mg/cm^3 was used as reference pristine silk (labeled "PS"). In order to alter, through accelerated aging, the secondary structure of fibroin and the mechanical properties of the silk fibers, three types of treatment were carried out on pristine silk. To induce changes by temperature, PS strips (10 $\times$ 15 cm^2) were heated in a convection oven at 130 °C for 4 h (samples labeled as "AS1"). To induce changes by acid hydrolysis, small PS strips (4 $\times$ 0.5 cm^2) were treated by dripping 10 μL of nitric acid (diluted to 1.8% v/v) over each PS sample, and then the samples were heated in a microwave oven at 570 W for 20 s (samples labeled as "AS2"). The microwave oven heating was meant to accelerate the reactions between nitric acid and fibroin (acid hydrolysis, oxidation, xanthoproteic reaction [50]), without using prolonged exposure to temperature and concentrated acid, which could lead to the complete destruction of the fibers. After the treatment, the samples were rinsed with MilliQ water and let dry at room temperature before analysis. To induce photo-oxidative degradation, PS strips (10 $\times$ 15 cm^2) were irradiated with UV–Vis light (samples labeled as "AS3"), as follows [48]: a Neon Light Color 765 Basic daylight Beghelli Lamp was used (160 mW/lm, 380-700 nm), placing the silk samples in a closed chamber for 30 days at room conditions (36 °C, RH 40%), where the samples' surface was exposed to ca. 11,000 Lux of homogeneous illumination. These conditions are meant to accelerate the natural aging that would be experienced by objects on display in museums, where illuminations of 50–100 lx are typically used.

2.3. Self-regenerated silk fibroin (SRSF) solutions

The SRSF solutions were obtained starting from waste scraps of Taffeta silk (density: 2.57 g/cm^3). The solutions were prepared following procedures reported in the literature [42,51]: the silk textiles were washed with ethanol four times to remove impurities and industrial additives, and let dry at room temperature; then, 0.5 g of textile was immersed in a 5 mL solution of CaCl$_2$:H$_2$O:EtOH (molar ratio of 1:8:2), heated at 60 °C and agitated until complete dissolution of the silk. The solution was then dialyzed with a membrane cell MC18 14 Kpa (Sigma Aldritch), against 1 L water (MilliQ) for two days, replacing the water after 1 h, 4 h, 10 h, 20 h, 32 h and 40 h. The dialyzed solution (12 mL, labeled as "initial") was centrifuged twice at 9000 rpm, and the supernatant separated. The final concentration is 5.34% (w/v). Two diluted solutions ("diluted", 1.18% w/v; "ultra-diluted", 0.15% w/v) were prepared from the initial solution. All the solutions were stored at 4 °C for 1 day before use.

2.4. SRSF coatings

A set of coated silk samples was prepared for each type of aged silk (AS1-3). Each set comprised small silk strips (4 $\times$ 0.5 cm^2) treated with, respectively, initial, diluted, or ultra-diluted SRSF solutions. The treatment consisted in dripping 15 μL of SRSF solution over the silk strip, taking care of wetting the fibers homogeneously so as to obtain a uniform coating. The coated samples were kept in a container at 22 °C and relative humidity (RH) of 43% for one week before analyses. The samples were labeled according to the received aging and coating treatment, e.g.: AS1-initial, AS1-diluted, AS1-ultra-diluted, AS2-initial, etc.

2.5. Fourier transform Infrared (FTIR) 2D Imaging-Chemical mapping

The SRSF films and the silk fibers (pristine, aged, and coated) were analyzed (without any pre-treatment) with a Cary 670 FTIR spectrophotometer coupled to a Cary 620 FTIR microscope (Agilent Technologies), using a 15x Cassegrain objective. Measurements were carried out in reflectance mode over a gold plated reflective surface; background spectra were collected directly on the gold-plated surface. Acquiring the spectra in reflectance mode was preferred to performing Attenuated Total Reflectance (ATR) on the films, as we previously showed that the pressure applied during ATR measurements might induce structural changes in the silk fibers, hindering the rigorous characterization of the films secondary structure via spectral deconvolution (peak fitting) [52]. The FTIR settings were as follows: 512 scans for each acquisition, spectral resolution of 2 cm^{-1}, open windows, and spectral range of 3900–900 cm^{-1}. A 128 $\times$ 128 pixels Focal Plane Array (FPA) detector was used (each pixel related to an area of 5.5 μm $\times$ 5.5 μm^2). Each analysis produced a "tile" of 700 $\times$ 700 μm^2. In the FTIR 2D maps, the chromatic scale shows the bands' intensity following the order red > yellow > green > blue.

2.5.1. Analysis of the secondary protein structures

An IR map was collected on a chosen spot of the SRSF films or silk fibers. Then, from each map, five spectra with high amide A absorbance, and fifteen spectra of the golden platelet were selected. The spectra of the Au surface where averaged to obtain a single spectrum, which was used as a reference to subtract environmental water absorptions from the spectra of the film/fiber. Then, each of the five film/fiber spectra underwent the following process: 1) Manual spectral subtraction of the reference Au spectrum; the subtraction factor was adjusted manually until no absorption at 1654 cm^{-1} (OH bending, H$_2$O) was observable in the spectra over the protein amide I band; 2) Smoothing with an SG quad-cubic function of 13–15 points, taking care not to alter any diagnostic feature of the spectra; 3) Spectrum truncation down to the 1720–1480 cm^{-1} range (amide I–II region); 4) Baseline correction using a linear function connecting the two extremes of the truncated spectra; 5) Each spectrum was normalized to the maximum absorbance value of the amide I band. Operations 1–5 were carried out using the Agilent Resolution Pro software (Agilent technologies). Each resultant spectrum was deconvoluted and fitted using the multipeak fitting package of the Igor Pro software, version 7 (WaveMetrics, Inc). First, the second derivative of the convoluted spectra was used to locate the position of bands. Then, the spectra were deconvoluted using Gaussian curves and a constant baseline (constrained at zero absorbance), in two steps: 1) The position and width of the bands were hold; the height of all bands was constrained to a maximum of 80 and a minimum of 0; the fitting was then iterated until no changes were reported between two successive iterations; 2) The width was let change in the 0–20 limit, and the height was let change with a minimum limit of 0; the fitting was iterated until no changes were reported between

two successive iterations. The resultant deconvoluted bands of amide I were assigned to the different secondary structures of the protein as follows [53,54]: (Tyr) side chains/aggregated strands, 1605–1615 cm^{-1}; aggregate β-strand/intermolecular β-sheets (weak), 1616–1621 cm^{-1}; intermolecular β-sheets (strong), 1622–1627 cm^{-1}; intramolecular β-sheets (strong), 1628–1637 cm^{-1}; random coils/extended chains, 1638–1646 cm^{-1}; random coils, 1647–1655 cm^{-1}; α-helices, 1656–1662 cm^{-1}; β-turns, 1663–1670, 1671–1685, and 1686–1696 cm^{-1}; intermolecular β-sheets (weak), 1697–1703 cm^{-1}; oxidation bands, 1703–1720 cm^{-1}.

2.6. Field emission scanning electron microscopy (FE-SEM)

FE-SEM investigation of the SRSF films and silk samples was carried out using a ΣIGMA instrument (Carl Zeiss Microscopy GmbH, Germany). Samples were gold coated, and images acquired using the secondary electron detector and in-lens secondary electron detector in an acceleration potential of 5 kV. For FE-SEM analyses, SRSF films were cast on glass slides by dripping 100 μL SRSF solution, and let dry in a desiccator at room temperature.

2.7. Differential scanning calorimetry (DSC)

A Q2000 DSC (TA Instruments, New Castle, DE, USA) instrument was used. Aluminum hermetic pans (TZero Aluminum Hermetic, TA Instruments) were used as sample holders and as a reference. The DSC measurements on the SRSF films were done using the following temperature program: initial isothermal for 2 min at 0℃, heat ramp of 10 ℃/min from 0℃ to 400℃, under nitrogen atmosphere (flow rate 50 mL/min). Reproducible results could be obtained using ca. 1 mg of silk sample for each measurement. The obtained data were elaborated with the Q Series software, version 5.4.0. Two measurements were carried out for each sample.

2.8. Tensile tests

Tensile measurements were performed at room conditions (T = 23℃, RH = 43%) with a Discovery HR-3 rheometer from TA Instruments, equipped with an extension accessory, recording the elongation and tensile force. The samples consisted of the silk textile PS, AS1-3, and their corresponding coated samples (initial, diluted, ultra-diluted); for each type, ten samples were tested, averaging the obtained values. Each sample contained 18 vertical threads of 100 μm diameter and 4 cm length. The gap length was set as 1 cm and the elongation speed set at 94 μm/s. Recorded data were transformed in strain strength values for analysis and discussion.

3. Results and discussion

Fig. 1 shows the FTIR 2D maps and SEM images of the SRSF films cast on glass slides (see Supplementary data for additional description). Significant differences in the shape of the amide I and II bands of the films were observed, ascribable to the presence of different secondary structures. The inset in Fig. 1 (panel 3) shows the 1729–1594 cm^{-1} region (amide I), where the intensity of the band component centered at 1644 cm^{-1} (random coils/extended chains [53]) was mapped. It is evident from the maps (Fig. 1, panels 1A-1C) that the content of amorphous structures follows a reverse trend with concentration, i.e. SRSF-initial < SRSF-diluted < SRSF-ultra-diluted. This feature is observed homogeneously all across the films' surface down to the micron scale.

The deconvolution of the amide I region detailed the differences in the secondary structure of the SRSF films cast from solutions at
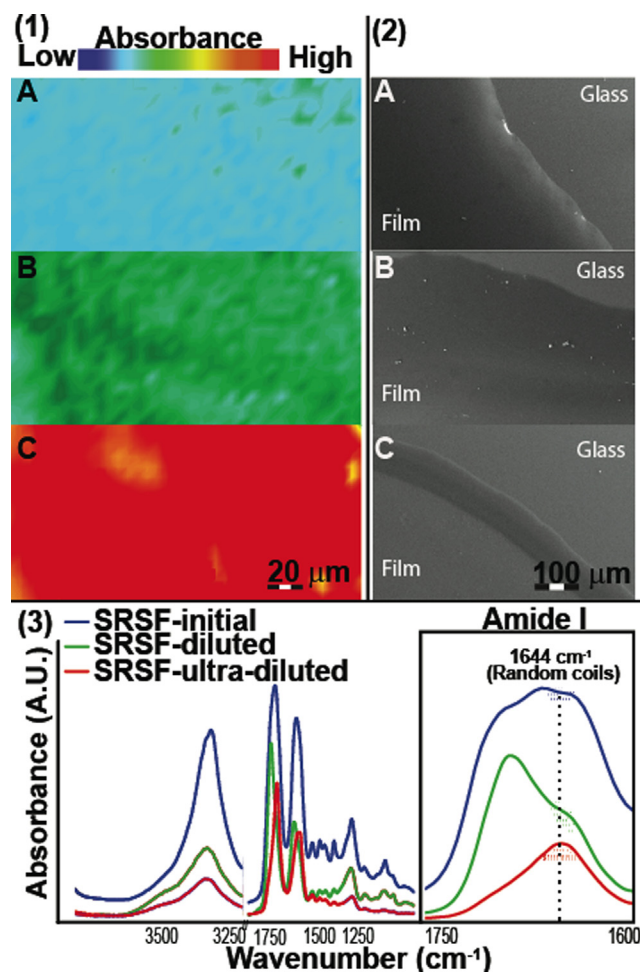

Fig. 1. FTIR 2D Imaging-Chemical mapping and SEM images of SRSF films cast from dispersions of waste silk. (1) FTIR 2D maps of the intensity of the 1652–1634 cm^{-1} region (amide I band, random coils/extended chains) for the SRSF-initial (A), SRSF-diluted (B), and SRSF-ultra-diluted (C) films. (2) SEM images of the SRSF-initial (A), SRSF-diuted (B), and SRSF-ultra-diluted (C) films cast on glass slides. (3) Representative examples of FTIR spectra, each corresponding to one pixel (5.5 × 5.5 μm^2) in the Imaging maps. The inset shows the 1750–1600 cm^{-1} region of the spectra (amide I), and the mapped portions of the peaks' areas (shaded areas, 1652–1634 cm^{-1}, centered at 1644 cm^{-1}).

different concentrations. The waste silk used to produce the films was considered as a reference to understand structural rearrangements due to solubilization and film formation. Results are shown in Fig. 2 (see Supplementary data for additional description). Intermolecular β-sheets decrease passing from waste silk to SRSF-initial and SRSF-diluted, and completely disappear in SRSF-ultra-diluted, where intramolecular β-sheets are also absent. α-helices are more present in SRSF-initial than in the original waste fabric, but disappear in SRSF-ultra-diluted. The total content of β-turn structures is similar for waste silk and SRSF-initial, but increases in SRSF-diluted, where β-turns are the main structure. SRSF-ultra-diluted shows β-turn contents similar to waste silk, but a dramatically higher content of random coils/extended chains, which are the main type of secondary arrangement in this film. Overall, we concluded that increasing the concentration of fibroin in the solutions leads to progressive ordering of the protein structure in the SRSF films, i.e. from random coils/extended chains to β-turns, α-helices, and eventually ordered β-sheets. β-turns seem to represent an intermediate step in the transition from highly amorphous to more crystalline films. Previously, Magoshi et al.[55] suggested that conformational change between random coils (or α-helices)

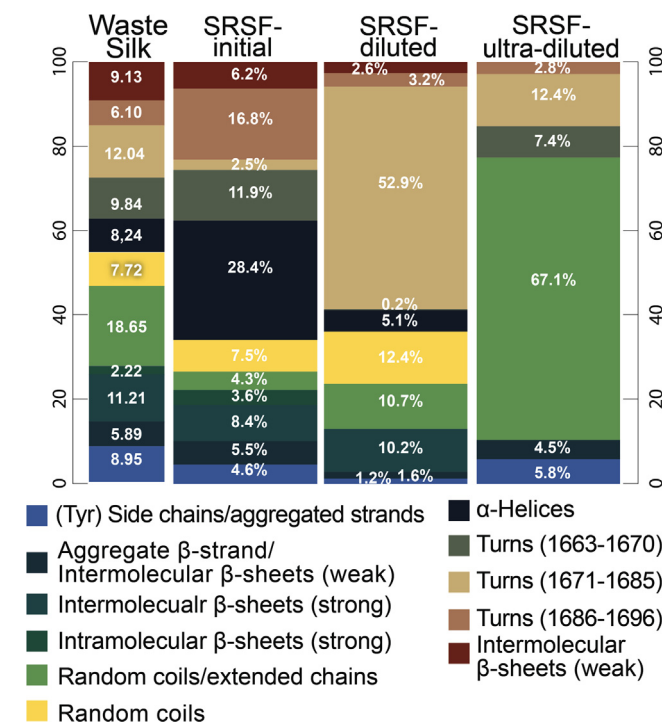**Fig. 2.** Assigned secondary structures (%) of silk protein, obtained from the deconvolution of the amide I and II region (1720–1480 cm^{-1}) of reflectance FPA μ-FTIR spectra of waste silk and SRSF films (initial, diluted, ultra-diluted). The deconvoluted bands, composing amide I, were assigned to the different secondary structures of the protein according to the bands' wavenumbers as explained in Section 2.5.1.

and β-sheets might occur by concentration variations in fibroin solutions (<3 wt%), even though no details of the effect of concentration on the conformation were given. Xie and Liang [56] carried out differential scanning calorimetry (DSC) and Raman spectroscopy on concentrated (15–37 wt%) regenerated silk fibroin aqueous solutions, and speculated that concentration increase resulted in close arrangement of the fibroin molecules and transition from random coil and α-helices to β-sheets. Models of transition from β-turns in un-spun silk I ('disordered') to β-sheets in spun silk II ('crystallized') have been proposed on the basis of NMR, X-ray diffraction, IR, circular dichroism, and Raman scattering [16], and Cheng et al. showed that silk I – silk II transition took place upon filmation of SRSF solutions [51]; the same authors also surmised that the size of the regenerated silk fibroin molecular weight is not intimately linked with its conformational transition.

The self-assembly of silk in aqueous solution is a thermodynamically driven process where kinetics also play a key role [57]. Lu et al. proposed a model of chain folding and micelle formation of the silk fibroin chain, where the long hydrophilic-hydrophobic-hydrophilic polymer folds into micelles (100–200 nm) via hydrophobic and hydrophilic interactions in aqueous solutions; the micelles can then assemble into nanofibrils or larger globules, depending on the drying conditions. In concentrated silk solutions, fibril formation is preferred since an approaching micelle is subjected to repulsive force from only one micelle, as opposed to stronger repulsion from multiple micelles when globules are formed [58]. If pH approaches the isoelectric point of fibroin (~4.2), micelles can aggregate to larger globules thanks to the shielding of negative charges. Key factors in the kinetics of the process include molecular mobility, hydrophilic/hydrophobic interactions, charge, and water content [58]. The energy barrier to form silk I from intermediate stages is lower than that needed for the silk I – silk II transition. The latter needs sufficient molecular

mobility in order to overcome the barrier resulting from hydrophilic silk-bound water interactions; controlling such interactions (e.g. by changing the drying time or adding glycerol) allows the production of different silk fibroin-based materials composed of silk I rather than silk II [58].

Further considerations on the mechanisms and kinetic effects involved in the formation of crystalline structures by the more concentrated SRSF samples, can also be made based on a hierarchical self-assembly model for peptides proposed by Aggeli et al. [59]. These authors tested a statistical mechanical model to describe the assembly of chiral rod-like units, e.g. β-sheet-forming peptides, into helical tapes, which with increasing concentration associate into twisted ribbons (double tapes), fibrils (twisted stacks of ribbons), and fibers (entwined fibrils). Initially, rod-like "monomers" self-assemble via recognition between complementary donor and acceptor groups to form twisted tapes, which curve into a helical configuration. In turn, the chemical anisotropy (different hydrophobicity) of the two faces of the tape results in intertape attraction, forming double tapes (ribbons) that are mutually attractive via smaller energy, leading to stacks of ribbons (fibrils). Finally, the fibrils' edges can also be mutually attractive, causing fibrils to entwine into fibers. However, to aggregate, these units must adjust in response to packing constraints, i.e. there is an elastic energy cost that must be compensated for by the gain in attraction energy [59]. Eventually, it is such energy balance that determines, from a thermodynamic standpoint, the final self-assembled hierarchical structure; for high attraction energies, the ribbons can even form extended sheet-like crystallites. The random coil to β-sheet transition was reported to start abruptly at ca. 0.07 mM peptide concentration for the most associative type of peptide considered in the study (rich in glutamine, phenylalanine, and tryptophan), but such value can vary by orders of magnitude depending on the efficiency of intermolecular side-chain interactions. Interestingly, the transition mechanism was deemed as reminescent of the formation of micelles in surfactant solutions, or the stabilization of micelles by amphiphilic interactions [59], which nicely links with the fibroin micelle self-assembly models discussed above. The kinetics of the random coil to β-sheet transition was likewise shown to be dependent on peptide concentration [59], with a timescale ranging from several weeks at low concentration, to several hours for concentrations of ca. 4 mM. This is in fairly good agreement with our observations, considering in our case the upper limit of 14 kDa (given by the molecular weight cut-off of the dialysis membrane), which would imply a ~ 3.8 mM concentration (53.4 g/L, 5.34% w/v) for the initial SRSF dispersion that produced the highest amount of β-sheet structures. It must be noticed that such concentration values are roughly three orders of magnitude larger than the critical overlapping concentration, C*, reported elsewhere for solutions of some heavier silk fibroin (~444 kDa) [60].

Finally, Yang et al. shed light on the link between silk molecules' surface activity and their self-assembly to form β-sheet rich SRSF films [61]. The chemical potential of the fibroin molecules increases with their bulk concentration, making the free energy of transfer of a molecule to the surface more favorable; surface adsorption continues until the chemical potential of the adsorbed molecules equals that in the bulk solution. In diluted solutions, the adsorption mechanism is mixed diffusion-kinetic controlled, probably because diffusion is faster than in concentrated solutions, where fibroin form larger, slow-diffusing aggregates, and the process is diffusion-controlled. Regenerated fibroin solutions exhibit constant surface tension beyond certain concentration values, again in agreement with the formation of aggregates in solution (e.g. micelles) [61]. After their adsorption at the air–water interface, the fibroin molecules continue to rearrange through interactions occurring both at the hydrophobic and hydrophilic side-chains. At low concentrations, they probably adopt a

stretched conformation, leading to the formation of compact multi-layers (molecules adsorbed below the first layer act cooperatively as anchors for incoming molecules from the bulk). Increasing the fibroin concentration, crowded adsorbed molecules are likely to extrude out of the surface, leading to a membrane of compact aggregates loosely interconnected. Overall, this description elucidated the formation of a two-dimensional physical fibroin gel at the air–water interface, with a soft glassy transitional behavior [61].

The DSC curves of the SRSF films are shown in Fig. 3 (see Supplementary data for additional description). The curve of SRSF-ultra-diluted exhibits features ascribable to amorphous fibroin domains, i.e. a broad pronounced peak of superimposing water evaporation and glass transition (30-160℃), and an exothermic peak (220℃) due to thermally induced random coil to β-sheet conformational transition [62–64]. The wide endothermic peak centered at 288℃ is due to the thermal degradation of the fibroin chains [65]. Instead, the curves of SRSF-initial and -diluted show features typical of more ordered structures: 1) a significantly weaker water loss event, consistent with the presence of crystalline domains where proteins' OH groups are largely involved in intramolecular bonds and thus less available to interact with free water [66,67]; 2) significantly weaker random coil to β-sheet transitions (215℃); 3) sharp endothermic peaks at ∼ 260℃, associated with the melting transition of the proteins (the peak of SRSF-initial is sharper and more intense than that of SRSF-diluted). Overall, thermal analysis supports FTIR data, indicating that the increase in fibroin concentration from SRSF-ultra-diluted to –initial progressively results in a rearrangement of the fibroin chains from amorphous (random coils, extended chains) into ordered structures (α-helices, β-sheets). Importantly, the film preparation can be feasibly tuned playing on the concentration of fibroin in the starting solutions, so as to obtain either highly amorphous (random coils/extended chains > 60%) or crystalline films (α-helices + β-sheets > 50%, without counting β-turns).

As mentioned in the introduction, the possibility of tuning the secondary structure of the SRSF films is attractive for the conservation of aged and degraded silk fibers, because crystalline or amorphous coatings are expected to produce different effects on the mechanical behavior of the treated fibers. Ideally, the SRSF dispersions should penetrate through the textile, adhere to the fibers, and create new film-fiber interfaces. Because the response of materials to mechanical loading is influenced and characterized by the presence and evolution of various interfaces [68], we expected that the aged silk fibers, once treated with the SRSF dispersions, would exhibit different mechanical behavior. Namely, films rich in crystalline domain should increase the stiffness of the fibers, while the adhesion onto the fibers of amorphous films (with more mobile fibroin chains) is expected to increase the fibers ductility. The concept of applying coatings with tunable composition to degraded textiles was also recently proposed for the conservation of canvases by Kolman et al., who combined polyelectrolyte-treated silica (SNP) to cellulose nanofibrils (CNF), varying the SNP/CNF ratio to balance the stiffness and ductility increase of the canvas fibers [69].

The degraded silk fibers considered in the present contribution were obtained starting from pristine commercial silk that was artificially aged using temperature, nitric acid, or UV–Vis light. These treatments were aimed to alter the secondary structure of the silk fibers and induce different changes in their mechanical behavior, prior to the application of the SRSF coatings. Fig. 4 shows the secondary structure of the commercial silk samples before and after aging treatments (see Supplementary data for additional description). Pristine commercial fibers (Georgette silk) have similar structural motifs to the waste silk used to prepare the SRSF films. UV–Vis aging produced a significant decrease of intramolecular

β-sheets and α-helices, and an increase of random coils/extended chains and β-turns; this indicates the formation of smaller crystallites (β-sheets), and the partial transformation of crystalline domains into less-ordered structures (random coils), as previously observed for photo-aged silk [48]. Treatment with nitric acid (sample AS2) resulted in the appearance of aggregate β-strand/intermolecular β-sheets (weak), the increase of β-turns, and the decrease of α-helices. The treatment also produced a significant yellowing of the sample. Thermally treated commercial silk (sample AS3) exhibited an increase of α-helices and a decrease of random coil structures.

The presence of different secondary structures in the aged silk allows making predictions on their mechanical behavior. In fact, both the tensile strength and the elongation length of silk fibers are intimately related to their secondary structure [47,70–72]. In general, lower crystallinity (β-sheets) implies lower strength and stiffness of the silk, but higher elasticity and toughness [47,70].

Table 1 shows the tensile strength, elongation length and Young's modulus of commercial fibers, either pristine, aged, or coated (after aging) with the SRSF dispersions. The stress–strain plots of the silk samples are reported in the Supplementary data.

Thermal aging caused some decrease in the elongation length, and an increase in tensile strength, in agreement with what observed with FTIR, i.e. the decrease in amorphous structures (random coil, extended chains) that provide mobility and ductility to the fibers. In fact, Tsukada et al. reported a decrease in ductility of the thermally treated fibers, which exhibit a slight contraction from room temperature to 120℃, attributed to the evaporation of humidity followed by a rearrangement of the structure [73]. The samples aged with nitric acid exhibit a high dispersion in the values of tensile strength, which are in average closer to those of pristine fibers than thermally and photo-aged samples. However, treatment with nitric acid produced the highest elongation length, consistently with the reduction of some ordered structures (α-helices) observed with FTIR. Photo-aging did not affect significantly the tensile strength, which remained similar to that of pristine samples, but decreased the fibers' elongation length, similarly to thermal aging. In fact, it has been reported that photo-aging of silk results in increased brittleness of the fibers [74,75]. This is in agreement with the presence of smaller crystalline domains observed with FTIR.

When the aged samples are treated with the SRSF dispersions, some general trends are observable in their mechanical behavior: treatment with SRSF-initial tends to reduce the elongation length of the fibers. Besides, a drastic decrease in the tensile strength is observed. The application of SRSF-diluted improves mechanical behavior, with closer elongation to pristine fibers, while the tensile strength is higher than that obtained after applying SRSF-initial, but still lower than pristine silk. The application of SRSF-ultra-diluted produced the best results in terms of recovering the fibers' original mechanical behavior: the treated fibers show higher elongation than pristine and aged samples, and tensile strength comparable to pristine silk. Macroscopically, the fibers treated with SRSF-ultra-diluted exhibited improved resistance to handling. The behavior of the SRSF-treated fibers could be explained considering that the application of the SRSF dispersions and their adhesion to the silk fibers lead to the formation of new interfaces between the fibers surface and the fibroin films, which produce different mechanical properties depending on the films' composition: the application of a highly ordered material with reduced amorphous content results in brittleness, while amorphous layers with mobile chains increase ductility.

Fig. 5 shows the FTIR 2D Imaging-Chemical mapping and the SEM images of pristine commercial textile after photo-aging and the application of the SRSF-ultra-diluted dispersion. Mapping the fibroin band at 1230 cm^{-1} (amide III in random coil conformation
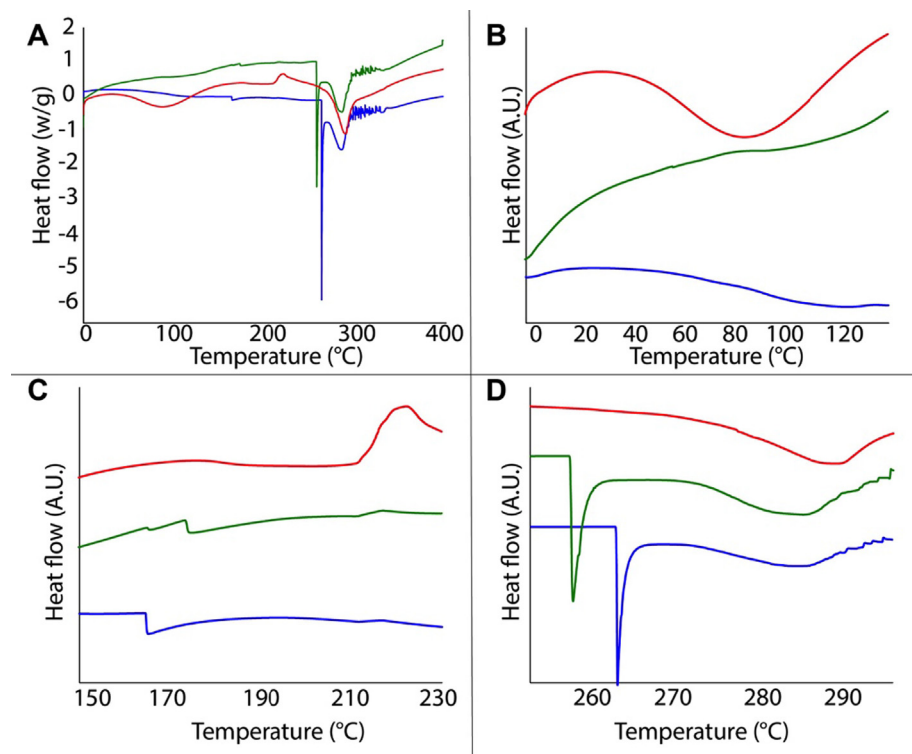
Fig. 3. (A) DSC curves of the SRSF films (SRSF-initial: blue curve; SRSF-diluted: green curve; SRSF-ultra-diluted: red curve). (B-D) Insets highlighting the three main thermal events observed for the SRSF films, in the 0-120℃ (loss of water), 150-230℃ (glass transition), and 250-300℃ (melting and protein decomposition).
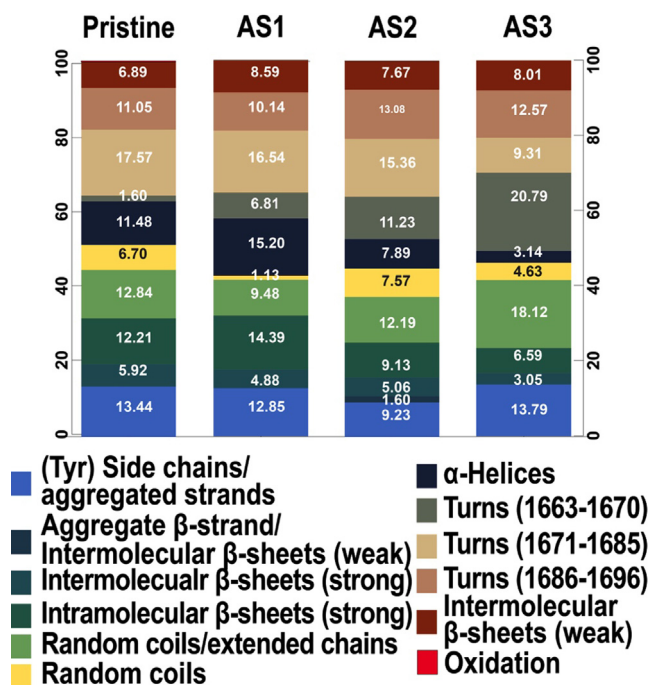

Fig. 4. Assigned secondary structures (%) of silk protein, obtained from the deconvolution of the amide I and II region (1720–1480 cm^{-1}) of reflectance FPA μ-FTIR spectra of commercial silk, either pristine or artificially aged with temperature (AS1), nitric acid (AS2), or UV–Vis light (AS3). The deconvoluted bands, composing amide I, were assigned to the different secondary structures of the protein according to the bands' wavenumbers as explained in Section 2.5.1.

[54,76]) shows that, following the application, the thread of fibers uniformly exhibits an increased amorphous content, without the presence of aggregates on the fibers or amorphous fibroin films

in the gaps between weft and warp. This suggests that the SRSF dispersion penetrates the textile and adheres homogeneously to the fibers, rather than simply creating a superficial layer, in good agreement with the improved mechanical behavior exhibited by the treated fibers.

4. Conclusions

We demonstrated that the composition of SRSF dispersions can be tuned, so as to obtain films with different secondary structures. Namely, it is possible to control the crystallinity Vs. amorphousness of the films, tuning the fibroin concentration in the dispersions (more concentrated dispersions progressively yield more crystalline films). When the SRSF dispersions are applied to aged silk fibers, domains with different degrees of order are formed between the fibers, changing their mechanical properties. We showed that the presence of amorphous domains, uniformly distributed between the fibers, completely recovered their mechanical properties, while domains with high content of ordered structures reduce the fibers' tensile strength and elongation length.

Our hypothesis was that the formation of new SRSF film-fiber interfaces would change the adhesivity of the fibers, producing different mechanical behaviors: SRSF domains with a significant amount of ordered structures (e.g. > 60%) were expected to increase the stiffness of the fibers, while films with reduced amount of ordered structures (e.g. < 30%) were expected to increase ductility (that is typically lost to degradation [17,48]). Previously formulated silk-fibroin composites involved embedding the silk fibers in thick coatings, so as to obtain significantly stronger fibers than pristine natural silk [43–47]. Instead, our goal was to avoid the formation of thick matrices, and to provide the *in situ* reinforcement (at the micro scale) of aged, degraded silk fibers, recovering their lost mechanical properties back to those of natural silk. This approach is a significant step forward with

Table 1
Elongation (%), tensile strength (MPa) and Young's modulus (MPa/mm) of commercial silk textiles, either pristine, artificially aged, or treated with SRSF after aging. Standard deviations (σ) are reported along with the average values (ten repeats were carried out for each sample). AS1: thermally aged silk; AS2: silk aged with nitric acid; AS3: silk aged with UV–Vis light. The labels "initial", "diluted", and "ultra-diluted" refer to the type of SRSF dispersions applied onto the textiles; fibroin concentration decreases passing from SRF-initial to SRF-ultra-diluted, and the dispersions yield fibroin domains where the arrangement of the fibroin chains changes from ordered (α-helices + β-sheets > 50%, without counting β-turns) to amorphous (random coils/extended chains > 60%). "AS1-initial" indicates thermally aged silk that was treated with the SRSF-initial dispersion, etc.

| Sample	Elongation		Tensile strength		Young's modulus	
	%	σ	MPa	σ	MPa/mm	σ
Pristine	50	4	158	13	422	41
AS1	41	5	189	16	630	30
AS1-initial	42	3	107	8	309	33
AS1-diluted	51	5	122	15	282	31
AS1-ultra-diluted	66	8	148	31	351	81
AS2	63	4	161	15	444	94
AS2-initial	47	10	101	22	287	34
AS2-diluted	54	7	121	19	344	37
AS2-ultra-diluted	64	10	141	29	351	49
AS3	40	3	149	11	431	20
AS3-initial	29	3	94	8	365	53
AS3-diluted	35	3	102	12	367	36
AS3-ultra-diluted	50	3	134	10	374	56
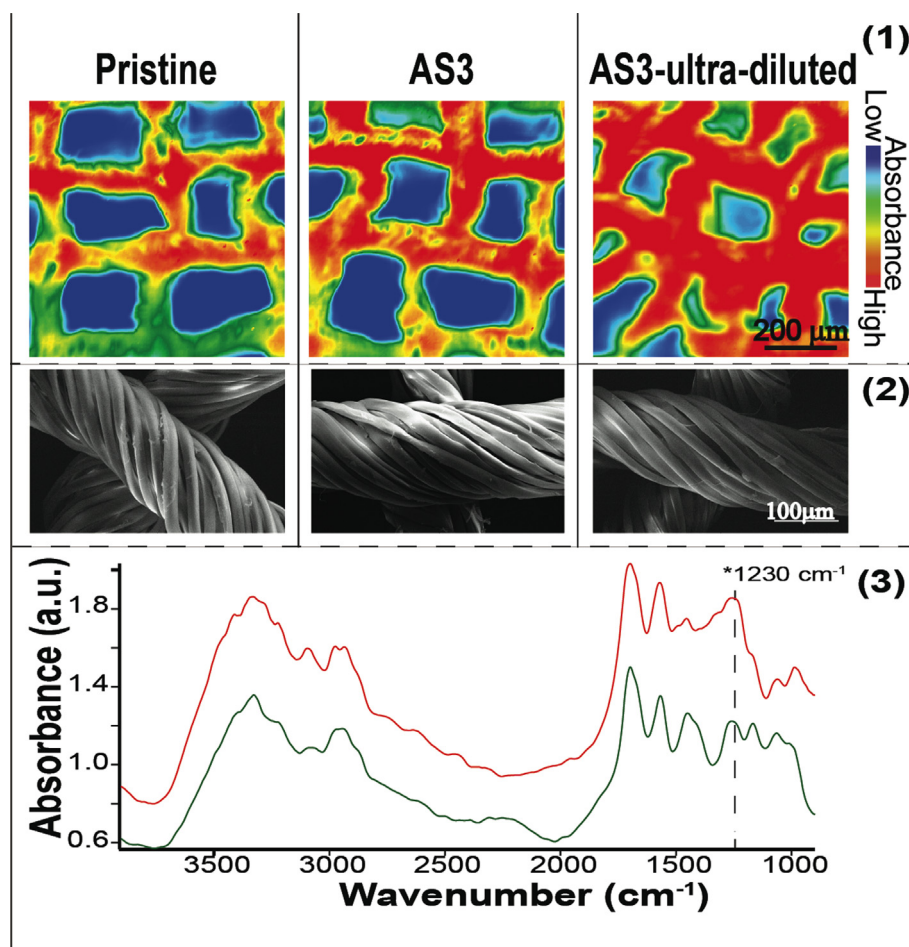
Fig. 5. (1) FTIR 2D Imaging-Chemical mapping of silk textiles: (left) pristine textile; (center) textile artificially aged with UV–Vis light (AS3); (right) the artificially aged textile after treatment with SRSF-ultra-diluted. The intensity of the 1230 cm^{-1} peak is shown (amide III, random coil conformation). (2) SEM images of the same textiles as in (1). Both FTIR 2D Imaging and SEM confirmed that SRSF-ultra-diluted distributes homogeneously within the fibers, without forming a superficial coating. (3) Representative examples of FTIR spectra, each corresponding to one pixel (5.5 × 5.5 μm^2) in the Imaging maps. Red and green spectra relate to pixels of the same color in the maps. The intensity of the 1230 cm^{-1} peak is highlighted.

respect to traditional textile conservation methods, which rely on repairs or synthetic adhesives that lack physico-chemical compatibility with the silk artifacts [25–28].

We showed that the increase in fibroin concentration of SRSF dispersions progressively produces a rearrangement of the fibroin chains from amorphous (films with random coils/extended chains > 60%) to crystalline films (films with α-helices + β-sheets > 50%, without counting β-turns). When the dispersions are applied to artificially aged and degraded silk textiles, they penetrate through the textile matrix, as showed by electron microscopy and 2D FTIR Imaging, adhering homogeneously to the fibroin fibers rather than forming a superficial layer. Treatment with concentrated SRSF dispersions (that yield ordered fibroin domains) tends to reduce the elongation length of aged silk fibers. Besides, a drastic decrease in the tensile strength is observed. Progressively lowering the concentration of the dispersions results in a better mechanical behavior of the treated fibers, with elongation values closer to those of pristine fibers, and some improvement of tensile strength (still lower than pristine silk). The best results were obtained applying the dispersion with the lowest fibroin concentration among the tested formulations: the treated fibers show higher elongation than pristine and aged silk samples, and tensile strength values comparable to pristine silk. These findings are in agreement with the hypothesis that the formation of new film-fiber interfaces changes the adhesivity of the fibers, producing different mechanical behaviors depending on the presence of mobile (amorphous) or brittle (crystalline) domains between the fibers.

Overall, we demonstrated that the secondary structure of SRSF films, obtained from renewable silk waste, can be easily tuned to confer desired mechanical properties to degraded silk fibers. These results open new perspectives in the conservation of textiles, where feasible consolidation materials are still largely needed. Besides, the use of SRSF films with tunable secondary structure is potentially useful in other fields such as biomaterials and materials engineering, and the preparation of composites with enhanced properties.

CRediT authorship contribution statement

David Chelazzi: Conceptualization, Methodology, Investigation, Writing - original draft, Writing - review & editing. **Diego Badillo-Sanchez:** Conceptualization, Methodology, Investigation, Writing - original draft, Writing - review & editing. **Rodorico Giorgi:** Conceptualization, Supervision. **Alessandra Cincinelli:** Conceptualization, Supervision. **Piero Baglioni:** Conceptualization, Supervision, Methodology, Writing - review & editing, Project administration.

Data availability

All the data to reproduce these findings are either included in the manuscript or in the supplementary material.

Declaration of Competing Interest

The authors declare that they have no known competing financial interests or personal relationships that could have appeared to influence the work reported in this paper.

Acknowledgements

Appendix A. Supplementary data

Supplementary data to this article can be found online at https://doi.org/10.1016/j.jcis.2020.04.114.

References

[1] N. Luxford, Silk durability and degradation, in: P.A. Annis (Ed.), Understanding and Improving the Durability of Textiles, Woodhead Publishing Limited, Cambridge, 2012, pp. 205–232. http://discovery.ucl.ac.uk/1366005/ (accessed December 1, 2016).

[2] F. Vollrath, D. Porter, C. Dicko, 5 - The structure of silk, in: Handbook of Textile Fibre Structure, Woodhead Publishing, 2009: pp. 146–198. // www.sciencedirect.com/science/article/pii/B9781845697303500056 (accessed January 26, 2017).

[3] S.K. Vyas, S.R. Shukla, Comparative study of degumming of silk varieties by different techniques, The Journal of The Textile Institute. 107 (2016) 191–199, https://doi.org/10.1080/00405000.2015.1020670.

[4] Á. Tímár-Balázsy, D. Eastop, Chemical principles of textile conservation, Butterworth-Heinemann, Oxford, 2004. https://trove.nla.gov.au/version/8460266 (accessed March 4, 2019).

[5] S. Inoue, K. Tanaka, F. Arisaka, S. Kimura, K. Ohtomo, S. Mizuno, Silk Fibroin of Bombyx mori Is Secreted, Assembling a High Molecular Mass Elementary Unit Consisting of H-chain, L-chain, and P25, with a 6:6:1 Molar Ratio, J. Biol. Chem. 275 (2000) 40517–40528, https://doi.org/10.1074/jbc.M006897200.

[6] M. Wojcieszak, A. Percot, S. Noinville, G. Gouadec, B. Mauchamp, P. Colomban, Origin of the variability of the mechanical properties of silk fibers: 4, Order/crystallinity along silkworm and spider fibers, Journal of Raman Spectroscopy. 45 (2014) 895–902, https://doi.org/10.1002/jrs.4579.

[7] D. Kaplan, W.W. Adams, B. Farmer, C. Viney (Eds.), Silk Polymers, American Chemical Society, Materials Science and Technology, 1994. http://gen.lib.rus.ec/book/index.php?md5=46294b434882f15d3cec192f62b11d22.

[8] R.S. Weber, C.L. Craig (auth.), T. Asakura, T. Miller (eds.), Biotechnology of Silk, 1st ed., Springer Netherlands, 2014. http://gen.lib.rus.ec/book/index.php?md5=f44d613bf7bb1ca80774ed6fcad3a90f.

[9] M. Farokhi, F. Mottaghitalab, Y. Fatahi, M.R. Saeb, P. Zarrintaj, S.C. Kundu, A. Khademhosseini, Silk fibroin scaffolds for common cartilage injuries: Possibilities for future clinical applications, Eur. Polym. J. 115 (2019) 251–267, https://doi.org/10.1016/j.eurpolymj.2019.03.035.

[10] P. Wongpanit, N. Sanchavanakit, P. Pavasant, T. Bunaprasert, Y. Tabata, R. Rujiravanit, Preparation and characterization of chitin whisker-reinforced silk fibroin nanocomposite sponges, Eur. Polym. J. 43 (2007) 4123–4135, https://doi.org/10.1016/j.eurpolymj.2007.07.004.

[11] P.J. Babu, M. Doble, A.M. Raichur, Silver oxide nanoparticles embedded silk fibroin spuns: Microwave mediated preparation, characterization and their synergistic wound healing and anti-bacterial activity, J. Colloid Interface Sci. 513 (2018) 62–71, https://doi.org/10.1016/j.jcis.2017.11.001.

[12] L. Yang, Z. Zheng, C. Qian, J. Wu, Y. Liu, S. Guo, G. Li, M. Liu, X. Wang, D.L. Kaplan, Curcumin-functionalized silk biomaterials for anti-aging utility, J. Colloid Interface Sci. 496 (2017) 66–77, https://doi.org/10.1016/j.jcis.2017.01.115.

[13] J. Chen, G. Cheng, R. Liu, Y. Zheng, M. Huang, Y. Yi, X. Shi, Y. Du, H. Deng, Enhanced physical and biological properties of silk fibroin nanofibers by layer-by-layer deposition of chitosan and rectorite, J. Colloid Interface Sci. 523 (2018) 208–216, https://doi.org/10.1016/j.jcis.2018.03.093.

[14] F. Vilaplana, J. Nilsson, D.V.P. Sommer, S. Karlsson, Analytical markers for silk degradation: comparing historic silk and silk artificially aged in different environments, Anal Bioanal Chem. 407 (2014) 1433–1449, https://doi.org/10.1007/s00216-014-8361-z.

[15] P. Colomban, H.M. Dinh, A. Bunsell, B. Mauchamp, Origin of the variability of the mechanical properties of silk fibres: 1 - The relationship between disorder, hydration and stress/strain behaviour, J. Raman Spectrosc. 43 (2012) 425–432, https://doi.org/10.1002/jrs.3044.

[16] V. Jauzein, P. Colomban, 6 - Types, structure and mechanical properties of silk, in: A.R. Bunsell (Ed.), Handbook of Tensile Properties of Textile and Technical Fibres, Woodhead Publishing, 2009: pp. 144–178. // www.sciencedirect.com/science/article/pii/B9781845693879500060 (accessed January 26, 2017).

[17] P. Garside, P. Wyeth, Crystallinity and degradation of silk: correlations between analytical signatures and physical condition on ageing, Appl. Phys. A. 89 (2007) 871–876, https://doi.org/10.1007/s00339-007-4218-z.

[18] P. Garside, S. Lahlil, P. Wyeth, Characterization of historic silk by polarized attenuated total reflectance Fourier transform infrared spectroscopy for informed conservation, Appl Spectrosc. 59 (2005) 1242–1247, https://doi.org/10.1366/000370205774430855.

[19] Y. Gong, L. Li, D. Gong, H. Yin, J. Zhang, Biomolecular Evidence of Silk from 8,500 Years Ago, PLoS ONE 11 (2016), https://doi.org/10.1371/journal.pone.0168042 e0168042.

[20] H.E. Ahmed, Y.E. Ziddan, A new approach for conservation treatment of a silk textile in Islamic Art Museum, Cairo, Journal of Cultural Heritage. 12 (2011) 412–419, https://doi.org/10.1016/j.culher.2011.02.004.

[21] Y. Nishio, Maintenance of Asian paintings II: minor treatment of scroll paintings, The Book and Paper, Group Annual 20 (2002). 15–26, ill.

[22] J.B. Perjés, K.E. Nagy, M. Tóth, Conserving Textiles Studies in honour of Ágnes Timár-Balázsy, ICCROM Conservation Studies 7, ICCROM, Italy, 2009.

[23] O.M.A. Abdel-Kareem, The long-term effect of selected conservation materials used in the treatment of museum artefacts on some properties of textiles, Polym. Degrad. Stab. 87 (2005) 121–130, https://doi.org/10.1016/j.polymdegradstab.2004.07.014.

[24] D. Chelazzi, A. Chevalier, G. Pizzorusso, R. Giorgi, M. Menu, P. Baglioni, Characterization and degradation of poly(vinyl acetate)-based adhesives for canvas paintings, Polym. Degrad. Stab. 107 (2014) 314–320, https://doi.org/10.1016/j.polymdegradstab.2013.12.028.

[25] O. Chiantore, M. Lazzari, Photo-oxidative stability of paraloid acrylic protective polymers, Polymer 42 (2001) 17–27, https://doi.org/10.1016/S0032-3861(00)00327-X.

[26] M. Favaro, R. Mendichi, F. Ossola, S. Simon, P. Tomasin, P.A. Vigato, Evaluation of polymers for conservation treatments of outdoor exposed stone monuments. Part II: Photo-oxidative and salt-induced weathering of acrylic–silicone mixtures, Polym. Degrad. Stab. 92 (2007) 335–351, https://doi.org/10.1016/j.polymdegradstab.2006.12.008.

[27] M. Lazzari, O. Chiantore, Thermal-ageing of paraloid acrylic protective polymers, Polymer 41 (2000) 6447–6455, https://doi.org/10.1016/S0032-3861(99)00877-0.

[28] S.-Q. Wu, M.-Y. Li, B.-S. Fang, H. Tong, Reinforcement of vulnerable historic silk fabrics with bacterial cellulose film and its light aging behavior, Carbohydr. Polym. 88 (2012) 496–501, https://doi.org/10.1016/j.carbpol.2011.12.033.

[29] D. Huang, Z. Peng, Z. Hu, S. Zhang, J. He, L. Cao, Y. Zhou, F. Zhao, A new consolidation system for aged silk fabrics: Effect of reactive epoxide-ethylene glycol diglycidyl ether, React. Funct. Polym. 73 (2013) 168–174, https://doi.org/10.1016/j.reactfunctpolym.2012.08.019.

[30] Z. Cai, G. Jiang, Y. Qiu, Chemical modification of Bombyx mori silk with epoxide EPSIB, J. Appl. Polym. Sci. 91 (2004) 3579–3586, https://doi.org/10.1002/app.13590.

[31] Y. Feng, X. Li, M. Li, D. Ye, Q. Zhang, R. You, W. Xu, Facile Preparation of Biocompatible Silk Fibroin/Cellulose Nanocomposite Films with High Mechanical Performance, ACS Sustainable Chem. Eng. 5 (2017) 6227–6236, https://doi.org/10.1021/acssuschemeng.7b01161.

[32] H.J. Kim, Y.J. Yang, H.J. Oh, S. Kimura, M. Wada, U.-J. Kim, Cellulose–silk fibroin hydrogels prepared in a lithium bromide aqueous solution, Cellulose 24 (2017) 5079–5088, https://doi.org/10.1007/s10570-017-1491-7.

[33] E. Marsano, P. Corsini, M. Canetti, G. Freddi, Regenerated cellulose-silk fibroin blends fibers, Int. J. Biol. Macromol. 43 (2008) 106–114, https://doi.org/10.1016/j.ijbiomac.2008.03.009.

[34] G. Yang, L. Zhang, Y. Liu, Structure and microporous formation of cellulose/silk fibroin blend membranes: I, Effect of coagulants, Journal of Membrane Science. 177 (2001) 153–161, https://doi.org/10.1016/S0376-7388(00)00467-1.

[35] L. Zhou, Q. Wang, J. Wen, X. Chen, Z. Shao, Preparation and characterization of transparent silk fibroin/cellulose blend films, Polymer 54 (2013) 5035–5042, https://doi.org/10.1016/j.polymer.2013.07.002.

[36] P. Ang-atikarnkul, A. Watthanaphanit, R. Rujiravanit, Fabrication of cellulose nanofiber/chitin whisker/silk sericin bionanocomposite sponges and characterizations of their physical and biological properties, Compos. Sci. Technol. 96 (2014) 88–96, https://doi.org/10.1016/j.compscitech.2014.03.006.

[37] S. Shang, L. Zhu, J. Fan, Intermolecular interactions between natural polysaccharides and silk fibroin protein, Carbohydr. Polym. 93 (2013) 561–573, https://doi.org/10.1016/j.carbpol.2012.12.038.

[38] D. Tian, T. Li, R. Zhang, Q. Wu, T. Chen, P. Sun, A. Ramamoorthy, Conformations and Intermolecular Interactions in Cellulose/Silk Fibroin Blend Films: A Solid-State NMR Perspective, J. Phys. Chem. B. 121 (2017) 6108–6116, https://doi.org/10.1021/acs.jpcb.7b02838.

[39] J.G. Hardy, L.M. Römer, T.R. Scheibel, Polymeric materials based on silk proteins, Polymer 49 (2008) 4309–4327, https://doi.org/10.1016/j.polymer.2008.08.006.

[40] S. Kapoor, S.C. Kundu, Silk protein-based hydrogels: Promising advanced materials for biomedical applications, Acta Biomater. 31 (2016) 17–32, https://doi.org/10.1016/j.actbio.2015.11.034.

[41] Y. Qi, H. Wang, K. Wei, Y. Yang, R.-Y. Zheng, I.S. Kim, K.-Q. Zhang, A Review of Structure Construction of Silk Fibroin Biomaterials from Single Structures to Multi-Level Structures, Int J Mol Sci. 18 (2017), https://doi.org/10.3390/ijms18030237.

[42] D.N. Rockwood, R.C. Preda, T. Yücel, X. Wang, M.L. Lovett, D.L. Kaplan, Materials Fabrication from Bombyx mori Silk Fibroin, Nat Protoc. 6 (2011), https://doi.org/10.1038/nprot.2011.379.

[43] Y. Duan, X. Chen, Z.-Z. Shao, The Silk Textile Embedded in Silk Fibroin Composite: Preparation and Properties, Chin J Polym Sci. 36 (2018) 1043–1046, https://doi.org/10.1007/s10118-018-2117-8.

[44] R.F.P. Pereira, M.M. Silva, V. de Zea Bermudez, Bombyx mori Silk Fibers: An Outstanding Family of Materials, Macromol. Mater. Eng. 300 (2015) 1171–1198, https://doi.org/10.1002/mame.201400276.

[45] M. Wojcieszak, A. Percot, P. Colomban, Regenerated silk matrix composite materials reinforced by silk fibres: Relationship between processing and mechanical properties, J. Compos. Mater. 52 (2018) 2301–2311, https://doi.org/10.1177/0021998317743563.

[46] Q. Yuan, J. Yao, X. Chen, L. Huang, Z. Shao, The preparation of high performance silk fiber/fibroin composite, Polymer, The International Journal for the Science and Technology of Polymers and Biopolymers. 51 (2010) 4843–4849, https://doi.org/10.1016/j.polymer.2010.08.042.

[47] S. Du, J. Zhang, W.T. Zhou, Q.X. Li, G.W. Greene, H.J. Zhu, J.L. Li, X.G. Wang, Interactions between fibroin and sericin proteins from Antheraea pernyi and Bombyx mori silk fibers, J. Colloid Interface Sci. 478 (2016) 316–323, https://doi.org/10.1016/j.jcis.2016.06.030.

[48] D. Badillo-Sanchez, D. Chelazzi, R. Giorgi, A. Cincinelli, P. Baglioni, Characterization of the secondary structure of degummed Bombyx mori silk in modern and historical samples, Polym. Degrad. Stab. 157 (2018) 53–62, https://doi.org/10.1016/j.polymdegradstab.2018.09.022.

[49] G.M. Nogueira, A.C.D. Rodas, C.A.P. Leite, C. Giles, O.Z. Higa, B. Polakiewicz, M.M. Beppu, Preparation and characterization of ethanol-treated silk fibroin dense membranes for biomaterials application using waste silk fibers as raw material, Bioresour. Technol. 101 (2010) 8446–8451, https://doi.org/10.1016/j.biortech.2010.06.064.

[50] G. Migliavacca, F. Ferrero, C. Tonin, Xanthoproteic reaction for the evaluation of wool antifelting treatments, Color. Technol. 130 (2014) 319–326, https://doi.org/10.1111/cote.12108.

[51] G. Cheng, X. Wang, S. Tao, J. Xia, S. Xu, Differences in regenerated silk fibroin prepared with different solvent systems: From structures to conformational changes, J. Appl. Polym. Sci. 132 (2015). n/a-n/a. 10.1002/app.41959.

[52] D. Badillo-Sanchez, D. Chelazzi, R. Giorgi, A. Cincinelli, P. Baglioni, Understanding the structural degradation of South American historical silk: A Focal Plane Array (FPA) FTIR and multivariate analysis, Sci. Rep. 9 (2019) 1–10, https://doi.org/10.1038/s41598-019-53763-5.

[53] X. Hu, D. Kaplan, P. Cebe, Determining Beta-Sheet Crystallinity in Fibrous Proteins by Thermal Analysis and Infrared Spectroscopy, Macromolecules 39 (2006) 6161–6170, https://doi.org/10.1021/ma0610109.

[54] J. Kong, S. Yu, Fourier Transform Infrared Spectroscopic Analysis of Protein Secondary Structures, Acta Biochim. Biophy. Sin. 39 (2007) 549–559, https://doi.org/10.1111/j.1745-7270.2007.00320.x.

[55] J. Magoshi, S. Nakamura, Physical properties and structure of silk. VIII. Effect of casting temperature on conformation of wild silk fibroin films, Journal of Polymer Science: Polymer Physics Edition. 23 (1985) 227–229, https://doi.org/10.1002/pol.1985.180230120.

[56] F. Xie, H. Liang, Effect of Concentration on Structure and Properties of Concentrated Regenerated Silk Fibroin Solution, in: Advanced Materials and Processes: ADME 2011, Trans Tech Publications, 2011: pp. 1653–1656. https://doi.org/10.4028/www.scientific.net/AMR.311-313.1653.

[57] H.-J. Jin, D.L. Kaplan, Mechanism of silk processing in insects and spiders, Nature 424 (2003) 1057–1061, https://doi.org/10.1038/nature01809.

[58] Q. Lu, H. Zhu, C. Zhang, F. Zhang, B. Zhang, D.L. Kaplan, Silk Self-Assembly Mechanisms and Control From Thermodynamics to Kinetics, Biomacromolecules 13 (2012) 826–832, https://doi.org/10.1021/bm201731e.

[59] A. Aggeli, I.A. Nyrkova, M. Bell, R. Harding, L. Carrick, T.C.B. McLeish, A.N. Semenov, N. Boden, Hierarchical self-assembly of chiral rod-like molecules as a model for peptide β-sheet tapes, ribbons, fibrils, and fibers, PNAS 98 (2001) 11857–11862, https://doi.org/10.1073/pnas.191250198.

[60] X. Li, G. Deng, L. Ma, X. Lu, Interchain Overlap Affects Formation of Silk Fibroin Secondary Structures on Hydrophobic Polystyrene Surface Detected via Achiral/Chiral Sum Frequency Generation, Langmuir 34 (2018) 9453–9459, https://doi.org/10.1021/acs.langmuir.8b01194.

[61] Y. Yang, C. Dicko, C.D. Bain, Z. Gong, R.M.J. Jacobs, Z. Shao, A.E. Terry, F. Vollrath, Behavior of silk protein at the air–water interface, Soft Matter 8 (2012) 9705–9712, https://doi.org/10.1039/C2SM26054A.

[62] J. Magoshi, M. Mizuide, Y. Magoshi, K. Takahashi, M. Kubo, S. Nakamura, Physical properties and structure of silk. VI. Conformational changes in silk fibroin induced by immersion in water at 2 to 130°c, Journal of Polymer Science: Polymer Physics Edition. 17 (1979) 515–520, https://doi.org/10.1002/pol.1979.180170315.

[63] J. Magoshi, S. Nakamura, Studies on physical properties and structure of silk, Glass transition and crystallization of silk fibroin, Journal of Applied Polymer Science. 19 (1975) 1013–1015, https://doi.org/10.1002/app.1975.070190410.

[64] A. Motta, L. Fambri, C. Migliaresi, Regenerated silk fibroin films: Thermal and dynamic mechanical analysis, Macromolecular Chemistry and Physics. 203 (2002) 1658–1665, https://doi.org/10.1002/1521-3935(200207)203:10/11<1658::AID-MACP1658>3.0.CO;2-3.

[65] Y. Gotoh, M. Tsukada, T. Baba, N. Minoura, Physical properties and structure of poly(ethylene glycol)-silk fibroin conjugate films, Polymer 38 (1997) 487–490, https://doi.org/10.1016/S0032-3861(96)00665-9.

[66] D. Mohanta, S. Santra, G.N. Reddy, S. Giri, M. Jana, Residue Specific Interaction of an Unfolded Protein with Solvents in Mixed Water-Ethanol Solutions: A Combined Molecular Dynamics and ONIOM Study, J. Phys. Chem. A. 121 (2017) 6172–6186, https://doi.org/10.1021/acs.jpca.7b05955.

[67] K. Yazawa, K. Ishida, H. Masunaga, T. Hikima, K. Numata, Influence of Water Content on the β-Sheet Formation, Thermal Stability, Water Removal, and Mechanical Properties of Silk Materials, Biomacromolecules 17 (2016) 1057–1066, https://doi.org/10.1021/acs.biomac.5b01685.

[68] A.M. Dongare, A.M. Rajendran, R. Namburu, M. Dubey, Understanding mechanical behavior of interfaces in materials, J Mater Sci. 53 (2018) 5511–5514, https://doi.org/10.1007/s10853-018-2030-0.

[69] K. Kolman, O. Nechyporchuk, M. Persson, K. Holmberg, R. Bordes, Combined Nanocellulose/Nanosilica Approach for Multiscale Consolidation of Painting

Canvases, ACS Appl. Nano Mater. 1 (2018) 2036–2040, https://doi.org/10.1021/acsanm.8b00262.

[70] J. Pérez-Rigueiro, M. Elices, J. Llorca, C. Viney, Effect of degumming on the tensile properties of silkworm (Bombyx mori) silk fiber, Journal of Applied Polymer Science. 84 (n.d.) 1431–1437. https://doi.org/10.1002/app.10366.

[71] J. Pérez-Rigueiro, C. Viney, J. Llorca, M. Elices, Silkworm silk as an engineering material, J. Appl. Polym. Sci. 70 (1998) 2439–2447, https://doi.org/10.1002/(SICI)1097-4628(19981219)70:12<2439::AID-APP16>3.0.CO;2-J.

[72] Ph. Colomban, G. Gouadec, Raman and IR micro-analysis of high performance polymer fibres tested in traction and compression, Compos. Sci. Technol. 69 (2009) 10–16, https://doi.org/10.1016/j.compscitech.2007.10.034.

[73] M. Tsukada, G. Freddi, M. Nagura, H. Ishikawa, N. Kasai, Structural changes of silk fibers induced by heat treatment, J. Appl. Polym. Sci. 46 (1992) 1945–1953, https://doi.org/10.1002/app.1992.070461107.

[74] G.S. Egerton, The Mechanism of the Photochemical Degradation of Textile Material, J. Soc. Dyers Colour. 65 (1949) 764–780, https://doi.org/10.1111/j.1478-4408.1949.tb02558.x.

[75] R.L. Feller, Accelerated aging: photochemical and thermal aspects, Getty Conservation Institute (1994).

[76] M.A. Koperska, D. Pawcenis, J. Bagniuk, M.M. Zaitz, M. Missori, T. Łojewski, J. Łojewska, Degradation markers of fibroin in silk through infrared spectroscopy, Polym. Degrad. Stab. 105 (2014) 185–196, https://doi.org/10.1016/j.polymdegradstab.2014.04.008.